Journal of Basic Physical Research ISSN: 2141-8403 Prints, 2141-8411 Online
Vol.14, Issue 2, October, 2025, pp. 167 – 182, Available online at https://journals.unizik.edu.ng/jbpr/

APPLICATION OF ELECTRICAL METHOD FOR GEOPHYSICAL ASSESSMENT OF SUBSURFACE STRUCTURES CONTRIBUTING TO ROAD FAILURES IN SHAO-MALETE ROAD, KWARA STATE.

Ahmad Imam Abdulmajeed[1], *Gabriel Efomeh Omolaiye[1], Jimoh Ajadi[1], Sodiq Bamidele Adam[1]
[1]Department of Geology and Mineral Science, Kwara State University, Malete, Kwara State, Nigeria
abdulmajeedahmad22@gmail.com , gab_omolaiye@yahoo.co.uk , jimoh.ajadi@kwasu.edu.ng & adambahmidayle@gmail.com
***Corresponding Author:** +2348099664112 & gab_omolaiye@yahoo.co.uk

Abstract
This study applies the Electrical Resistivity Method using the Vertical Electrical Sounding (VES) technique to investigate and evaluate subsurface structures contributing to recurrent road failures along the Shao-Malete Road in Kwara State, Nigeria. A total of seventy-one (71) VES stations were conducted using the Schlumberger array to delineate the subsurface lithological variations and assess their influence on pavement stability. The interpretation resistivity data revealed a different subsurface layer's sequence consisting of lateritic topsoil, clayey-sand, sandy-clay, weathered basement and fresh basement. The reveal that the lateritic topsoil was found to be thin or discontinuous in several failed segments of VES 6-10, 12, 14, 16 and 21 locations, making these areas vulnerable to deformation under vehicular loads. The clayey and sandy-clay layers is also characterized by low to moderate resistivity values identified at shallow depths in VES 5, 11, 22, 35, 42, 51, 52, 58, and 62 locations, which indicate high moisture retention and swelling potential that further contribute to pavement weakening during the wet season. In addition, a thick and poorly consolidated weathered basement layer was delineated beneath some failed segments, contributing to reduced subgrade strength and the development of pavement distress such as cracks and potholes. This study demonstrates that subsurface heterogeneity and moisture-sensitive materials play significant roles in the observed road failures. It recommends integrating geophysical surveys in preconstruction assessments to guide subgrade stabilization and drainage design for sustainable road infrastructure.
Keywords: *Road Failure, Shao-Malete Road, Basement Complex, Electrical Resistivity Method, Vertical Electrical Sounding (VES).*

Introduction

Road transportation remains the dominant mode of transportation in many developing countries due to its affordability and extensive spatial coverage (Adagunodo et al., 2025; Rasol et al., 2022). In Nigeria, more than 70% of passenger and freight movement depends on road networks, making the performance and durability of road infrastructure critical to socioeconomic development. Despite substantial investment in road construction and rehabilitation, frequent road failures, including cracks, potholes, gullies, and complete pavement collapse, have become a major national concern, leading to economic losses, increased accident rates, and reduced accessibility (Fajana et al., 2024; Agati et al., 2023). These failures often occur shortly after construction or rehabilitation, suggesting that factors beyond surface construction deficiencies are involved (Adagunodo et al., 2025). While surface engineering deficiencies are frequently blamed, recent studies increasingly attribute road failures to unfavorable subsurface geological and geotechnical conditions that undermine pavement stability (Agbo et al., 2024; Agati et al., 2023; Ademila, 2022). Therefore, understanding these subsurface conditions is essential for developing sustainable road infrastructure (Rasol et al., 2022).

Over the years, geophysical methods have proven to be effective, non-invasive, and cost-efficient tools for subsurface characterisation in civil and environmental engineering applications. These techniques enable the identification of weak zones, clay-rich layers, and water-saturated horizons that predispose road pavements to failure (Alao et al., 2025; Alao et al., 2024; Fajana et al., 2024; Omolaiye et al., 2024; Ademila, 2022). Commonly applied

geophysical techniques include seismic refraction, ground-penetrating radar (GPR), magnetic, electromagnetic, and electrical resistivity methods, each offering specific advantages depending on site conditions and investigation objectives (Paweł et al., 2025; Rahimi et al., 2024; Alsharahi et al., 2021). Seismic refraction is effective for estimating elastic properties and depth to bedrock. Magnetic or electromagnetic methods are useful for mapping conductive or magnetic anomalies. The electrical resistivity method is particularly suitable for delineating near-surface heterogeneities and moisture-sensitive materials that critically influence road performance (Alao et al., 2025; Bamidele & Omojemite, 2025; Omolaiye et al., 2025; Oluyemoh et al., 2025).

The electrical resistivity method operates on the principle that different earth materials show varying abilities to conduct electrical current, mainly influenced by their mineral composition, porosity, fluid content, and degree of saturation (Akingboye, 2025; Oyinkuro and Wilson, 2025; Omolaiye et al., 2024; Rahimi et al., 2024). By injecting a known current into the ground and measuring the resulting potential difference, the electrical resistivity of the subsurface can be assessed, which aids in evaluating subsurface stability and strength. Among the different setups of this electrical resistivity method, the Vertical Electrical Sounding (VES) technique is especially useful for examining how resistivity changes with depth, thereby providing a vertical profile of subsurface layers (Omolaiye et al., 2025; Oyinkuro and Wilson, 2025; Adenika et al., 2018). This method is highly effective at detecting weak zones, clayey subgrades, and water-saturated layers, which are often linked to pavement instability and failure (Adenika et al., 2018).

The Shao-Malete Road serves as an important transportation corridor linking Shao town, Malete, and Kwara State University, which have suffered failures soon after repairs, particularly during the rainy season. These persistent failures suggest the influence of adverse subsurface conditions such as differential weathering, fractured basement structures, and variations in soil resistivity. However, detailed geophysical investigations addressing these subsurface controls remain limited along this corridor. Therefore, this study applies the electrical resistivity method using the VES technique to characterize subsurface structures contributing to road failures along the Shao-Malete Road. The results are expected to provide geophysical constrained insights into pavement failure mechanisms and to support the integration of subsurface investigations into road design, maintenance, and rehabilitation strategies for sustainable infrastructure development in similar geological settings.

Study Area

This study area is located within Moro Local Government Area, Kwara State, Nigeria. It is geographically between latitude 8.586868 - 8.709778° N and longitude 4.560062 - 4.466141° E, covering an approximate distance of 16.9 km, which is a road network that connects several communities, such as Asomu, Elemere, Igbo Oriku and Malete, from Shao Junction to Malete town, as shown in Figure 1. The area falls within a tropical climate with wet and dry seasons. The wet season occurs from March to September, with temperatures fluctuating between 25 °C and 30 °C, while the dry season occurs from October to March, with temperatures ranging from 33 °C to 34 °C, and the annual rainfall ranges between 1,318 mm and 1,430 mm (Ajadi et al., 2025; Yusuf et al., 2025). The terrain is generally gently undulating with elevations within 300 m above sea level, which is characterized by low relief features and scattered rocky outcrops that influence both surface drainage and runoff distribution (Yusuf et al., 2025).

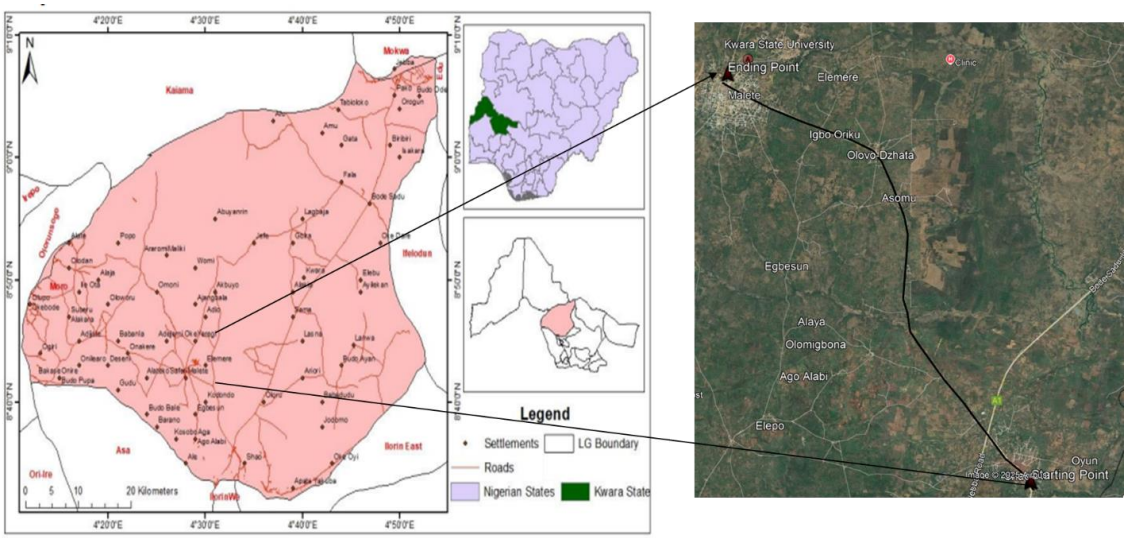

Fig. 1 *Map of the study Area showing Shao Junction to Malete, Kwara State.*

Geologically, Shao-Malete Road lies within the Precambrian Basement Complex of southwestern Nigeria, a component of the extensive Pan-African mobile belt (Ajadi et al., 2025; Oluyemoh et al., 2025; Yusuf et al., 2025). The study area is underlain by dominant lithological units including migmatite-gneiss complex, granite, quartzite and schist as shown in Figure 2, which occur as both outcrops and deeply weathered rocks structurally deforming and exhibiting fractures, joints and shear zones that influence subsurface stability (Ajadi et al., 2025; Yusuf et al., 2025). The degree of weathering is variable, producing layers of lateritic topsoil and clayey subsoil material underlain by fresh basement rock, which plays a significant role in the mechanical and hydrological behaviour of the subgrade materials along the road alignment.

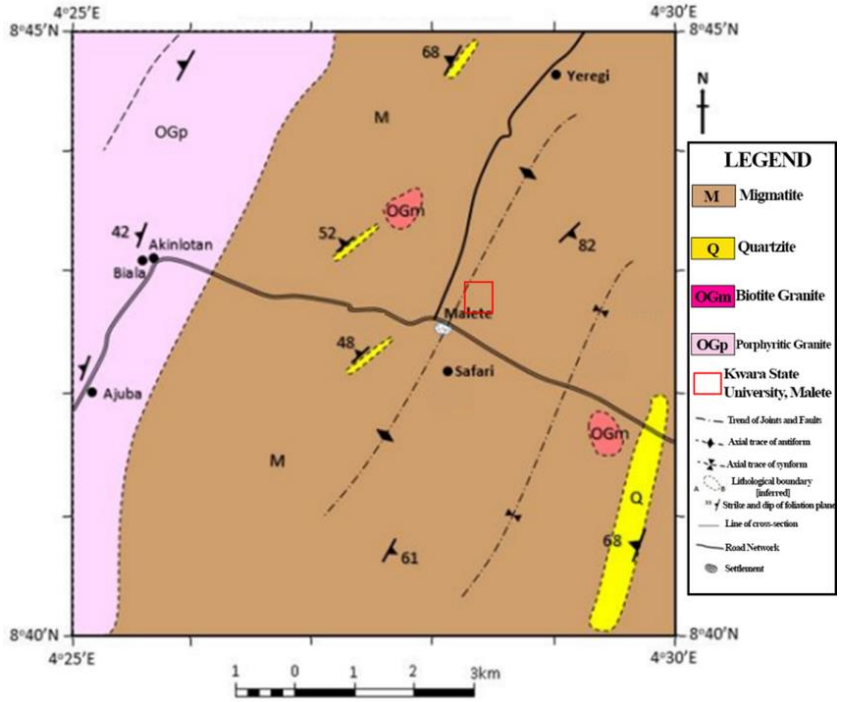

Fig. 2 Geologic map of Malete and its environment (Ajadi et al., 2025)

Materials and Methods

This study employed the Electrical Resistivity Method using the Schlumberger configuration of the Vertical Electrical Sounding (VES) technique to investigate the subsurface conditions along Shao-Malete Road that may cause or contribute to road failure in the study area. The primary instrument used for VES data collection was the HEROJAT Resistivity-meter, which measured subsurface resistance, supported by materials such as electrodes, insulated cables, hammers, measuring tapes, and a GPS reader. Figure 3 shows the field instrument and material used at the field location. A total of seventy-one (71) VES stations were established at regular intervals along Shao-Malete Road, strategically located across sections spanning 16.9 kilometres, with a maximum electrode spacing (AB/2) of 100 metres. The acquired field data were processed and interpreted using software such as Microsoft Excel for data computation, organisation, and preliminary analysis, and IPI2WIN to determine layer resistivities and thicknesses.

Fig. 3 Researcher and field instruments during VES survey for road failure investigation within the study area.

The Electrical Resistivity Method is the most commonly used geophysical technique for investigating near-subsurface lithological properties for various purposes, such as groundwater exploration and site assessments for buildings and roads. The Electrical Resistivity method is based on Ohm's Law Principle as shown in equations below, which involves introducing a known electrical current into the subsurface via a pair of current electrodes and measuring the resulting potential difference between pairs of potential electrodes placed on the surface. The measured potential difference and injected current are then used to calculate the apparent resistivity of the subsurface materials, as shown in equations 3 and 4 (Akingboye, 2025; Oyinkuro & Wilson, 2025).

$$\boldsymbol{V = I * R} \qquad \text{Eqn. 1}$$

$$\boldsymbol{R = \frac{V}{I}} \qquad \text{Eqn. 2}$$

$$\boldsymbol{\rho_a = R * G} \qquad \text{Eqn. 3}$$

$$\boldsymbol{G = \pi\left[\frac{\left[\left(\frac{AB}{2}\right)^2 - \left(\frac{MN}{2}\right)^2\right]}{MN}\right]} \qquad \text{Eqn. 4}$$

Where $\boldsymbol{\rho}$ is Voltage, **I** is Current, **R** is resistance value, $\boldsymbol{\rho_a}$ is the apparent resistivity, **G** is the geometric factor of Schlumberger electrode configuration, **AB** is the current electrode spreading distance, and **MN** is the potential electrode spreading distance.

Furthermore, among several electrode configurations, such as Wenner, Dipole-Dipole, and others, the Schlumberger configuration using the Vertical Electrical Sounding technique was employed in this study along Shao-Malete Road. The field survey involved arranging two current electrodes (A and B) to inject current into the ground at varying distances (spacings) along the road in a straight line, along with two potential electrodes to measure the potential difference in the subsurface. The central point of the electrodes remained fixed. In contrast, the spacing between the current and potential electrodes was increased from 1 m to 100 m to probe different subsurface depths and measure resistance at each spacing or depth. The maximum half-current electrode spacing (AB/2) of 100 m was selected to achieve adequate depth penetration required to image the subgrade, weathered basement, and shallow fresh basement layers that influence road performance. Additionally, data quality control was implemented during acquisition and processing. The calculated apparent resistivity values were inverted using IPI2WIN 1-D inversion modelling software to produce geoelectric profiles of the study area.

Results

Table 1 shows the results of all seventy-one (71) Vertical Electrical Sounding (VES) investigations of the Shao-Malete Road subsurface data, outlining different subsurface resistivity values, depths, and thicknesses after processing. The results show that the subsurface layers within the study area consist of three to five lithological units along the Shao-Malete Road, including Lateritic topsoil/Laterite, Clayey-sand, Sandy-clay, Weathered Basement, and Fresh Basement. The interpreted geoelectric studies indicate that the lateritic topsoil is the most dominant surface layer across the study area, with thicknesses ranging from 0.2 m to 2.0 m and resistivity values from 120 Ωm to 850 Ωm. Beneath this topsoil layer, clayey-sand and sandy-clay formations occur at intermediate depths, characterized by moderate resistivity values of 40 Ωm to 250 Ωm, suggesting mixed lithologies with varying clay and sand contents. These intermediate layers show considerable spatial variation in both thickness and resistivity, reflecting different weathering and depositional conditions along the investigated roadside.

Furthermore, the weathered basement layer was mapped at greater depths, showing resistivity values between 200 Ωm and 900 Ωm, indicating a composition of disintegrated and fractured bedrock materials with varying clay content. The thickness of this layer reaches approximately 12 m in some areas, reflecting uneven weathering. The fresh basement rock lies beneath this zone, characterised by high resistivity values exceeding 1000 Ωm, corresponding to compact, unweathered crystalline bedrock. The depth to the fresh basement varies significantly from about 2.5 m to 58 m, indicating considerable lateral variation and structural irregularity across the profile.

Figures 4, 5, and 6 show the geoelectric sections for the VES-inferred lithological units of the subsurface. Figure 6 displays examples of the IPI2WIN resistivity-depth plot images for some of the VES data results. Additionally, Table 1 presents various curve types, such as QH, H, HK, KQH, KHK, KQQ, HKH, QQH, KHH, QHH, and QHH, for all 71 VES data, with QH being the most common, as shown in the figure.

Table 1: Data results of VES 1 to 71 along the study area

VES No	**Layer No**	**Curve Type**	**Resistivity (Ω-m) $p_1/\ldots/p_i$**	**Thickness (m) $t_1/\ldots/t_i$**	**Depth (m) $d_1/\ldots/d_i$**	**Proposed Lithology type**
1	4	QH	2462/685/77.1/19755	1.08/ 2.74/ 3.29	1.08/3.82/ 7.11	Lateritic Topsoil/Sand/ Weathered Basement/Fresh Basement
2	3	H	1615/314/13512	1.58/5.73	1.58/7.31	Lateritic Topsoil/Sand/ Fresh Basement
3	4	QH	2535/1150/81.8/82390	1.8/4.06/ 6.3	1.8/5.86/ 12.2	Lateritic Topsoil/Laterite/ Weathered Basement/Fresh Basement
4	4	QH	2095/1039/124/130000	1.01/9.67/ 11	1.01/10.7/ 21.7	Lateritic Topsoil/Laterite/ Weathered Basement/Fresh Basement
5	3	H	81.6/29.3/82266	0.345/ 2.19	0.345/2.54	Clayey Topsoil/Weathered Basement/Fresh Basement
6	4	QH	2267/6579/466.9/11222	0.891/0.56/14.8	0.891/1.45/ 16.25	Topsoil/Laterite/Fractured Basement/Fresh Basement
7	4	QH	1610/460/148/ 39856	0.665/2.45/4.97	0.665/3.12/8.02	Lateritic Topsoil/Sandy Clay/Weathered Basement/Fresh Basement
8	5	HKH	1629/ 441/ 1909/91.9/ 260000	0.708/1.79/2.72/6.16	0.708/2.5/5.22/ 11.4	Lateritic Topsoil/Sand/Dry Laterite/ Weathered Basement/Fresh Basement
9	4	QH	5089/272/57/ 29125	0.355/1.46/5.19	0.355/1.81/7	Lateritic Topsoil/Clayed Sand/ Weathered Basement/Fresh Basement
10	4	QH	1242/360/94.3/71428	0.528/3.89/4.67	0.528/4.41/9.08	Lateritic Topsoil/Sand/Weathered Basement/Fresh Basement
11	5	HK	1108/119/4997/140/99651	0.753/1.01/3.18/5.71	0.753/1.76/4.94/10.7	Topsoil/Sandy Clay/Laterite, Weathered Basement/Fresh Basement

12	4	QH	1071/523/140/370000	0.641/2.74/3.69	0.641/3.38/7.07	Lateritic Topsoil/Sand/Weathered Basement/Fresh Basement
13	4	H	730/133/14115/78.5	6.76/5.57/14.9	6.76/12.3/27.2	Topsoil/Clayey Sand/Fresh Basement/Fracture Basement
14	4	QH	1622/497/104/160000	0.902/2.95/6.14	0.902/3.85/9.99	Lateritic Topsoil/Sand/Weathered Basement/Fresh Basement
15	5	KQQ	5456/10479/975/310/410000	0.629/0.621/4.42/14.1	0.629/1.25/5.67/19.0	Compacted Topsoil/Laterite /Fracture Basement/Weathered Basement/Fresh Basement
16	5	HKH	1156/148/3533/119/1716	0.487/0.614/1.22/5.41	0.487/1.1/2.32/7.73	Lateritic Topsoil/Clayey Sand/ Fractured Basement/Weathered Basement/Fresh Basement
17	4	QH	4829/1100/163/7854	1.58/2.8/6.32	1.58/4.37/10.7	Lateritic Topsoil/Fractured Basement/Weathered Basement/Fresh Basement
18	5	KQH	1112/4126/934/269/2302	0.6/0.654/4.3/5.97	0.6/1.25/5.55/11.5	Topsoil/Laterite/Fractured Basement/Weathered Basement/ Fresh Basement
19	5	KHK	2282/8186/233/462/48.1	0.6/0.654/1.37/26.6	0.6/1.25/2.62/29.2	Topsoil/Compacted Laterite/ Weathered Basement/Fracture Basement
20	5	QQH	2077/1662/839/109/60901	0.6/2.05/8.86/12.5	0.6/2.65/11.5/24	Topsoil/Laterite/Fractured Basement/Weathered Basement/Fresh Basement
21	4	QH	1128/477/146/13076	0.82/2.6/13.3	0.82/3.42/16.7	Lateritic Topsoil/Sand/Weathered Basement/Fresh Basement
22	5	KHH	712/2628/142/23.7/4879	0.247/0.65/4.79/13.6	0.247/0.897/5.69/19.3	Topsoil/Laterite/Clayey Sand/Weathered Basement/Fresh Basement

23	4	HK	933/623.7/15223/48.16	0.8735/7.234/10.14	0.8735/8.108/18.25	Topsoil/Sand/Fresh Basement/ Weathered Basement
24	4	QH	1643/499.3/243.8/2252	1.554/3.234/7.798	1.554/4.788/12.59	Lateritic Topsoil/Fracture Basement/Fresh Basement
25	5	QHH	2651/1323/614/311.5/2273	0.6247/2.047/2.934/16.93	0.6247/2.672/5.606/22.54	Topsoil/Laterite/Fracture Basement/Fresh Basement
26	5	QQH	2799/1312/475/145.2/1526	0.7696/1.96/4.488/7.438	0.7696/2.73/7.218/14.66	Topsoil/Laterite/Sand/Weathered Basement/Fresh Basement
27	5	QKH	3411/1550/470/118/52772	0.48/1.62/7.07/12.3	0.48/2.1/9.17/21.5	Topsoil/Laterite/Sand/Weathered Basement/Fresh Basement
28	5	QQH	3913/2408/950.3/347/3883	0.6/2.031/8.83/12.48	0.6/2.631/11.46/23.94	Topsoil/Lateritic Soil/Fracture Basement/Fresh Basement
29	4	QH	2078/925/224/7320	1.33/5.1/10.1	1.33/6.44/16.6	Lateritic Topsoil/Sand/Weathered Basement/Fresh Basement
30	4	KH	1034/2040/320/120000	0.567/3.05/19.3	0.567/3.61/22.9	Topsoil/Laterite/Fractured Basement/Fresh Basement
31	4	QH	2121/947/226/6931	1.33/5.1/10.1	1.33/6.43/16.6	Lateritic Topsoil/Sand/Clayey Sand/Fresh Basement
32	5	KQH	2569/8012/985/357.6/12827	0.4326/0.6182/6.227/23.68	0.4326/1.051/7.278/30.96	Topsoil/Laterite/Fractured Basement/Fresh Basement
33	3	H	1618/56.8/2930	2.8/2.17	2.8/4.98	Lateritic Topsoil/weathered basement/Fresh Basement
34	4	QH	942/308/92.1/52150	0.795/3.15/5.9	0.795/3.95/9.85	Lateritic Topsoil/Sand/Weathered Basement/Fresh Basement
35	4	QH	873/148.1/43.08/7787	0.6647/1.943/2.831	0.6647/2.608/5.439	Topsoil/Clayey Sand/Weathered Basement/Fresh Basement

36	3	H	996/113/47139	0.491/7.12	0.491/7.61	Topsoil/Weathered Basement/Fresh Basement
37	5	KQH	2151/5625/625/192/5952	0.705/0.637/4.92/12.2	0.705/1.34/6.26/12.2	Topsoil/Compacted Laterite/Sand/ Weathered Basement/Fresh Basement
38	4	QH	1898/622/67.7/96782	0.494/2.02/2.68	0.494/2.52/5.2	Lateritic Topsoil/Sand/Weathered Basement/Fresh Basement
39	5	HKH	1843/510/914/374/4064	0.573/1.09/3/17.8	0.573/1.66/4.66/22.5	Topsoil/Sand/Laterite/Fractured Basement/Fresh Basement
40	5	QQH	2218/925/384/64.9/150000	0.344/1.36/4.04/5.98	0.344/1.7/5.74/11.7	Lateritic Topsoil/Fractured Basement/Weathered Basement/Fresh Basement
41	4	QH	3376/1351/245/180000	0.363/1.37/15.8	0.363/1.73/17.5	Compacted Lateritic Topsoil/ Laterite/Weathered Basement/Fresh Basement
42	4	HK	1225/182/39396/175	1.43/8.56/10.4	1.43/9.99/20.4	Lateritic Topsoil/Clayey Sand/Fresh Basement/Fracture Basement
43	4	QH	2623/1116/159/11000000	0.315/1.2/18.3	0.315/1.52/19.8	Compacted Lateritic Topsoil/ Laterite/Weathered Basement/Fresh Basement
44	3	H	2007/397/88641	6.98/34.1	6.98/41.1	Lateritic Topsoil/Fractured Basement/Fresh Basement
45	4	QH	3003/663/205/78139	2.18/5.83/11	2.18/8.01/19	Lateritic Topsoil/Sand/Weathered Basement/Fresh Basement
46	4	QH	2053/470/101/9436	0.95/3.37/5.17	0.95/4.32/9.49	Lateritic Topsoil/Sand/Weathered Basement/Fresh Basement
47	4	QH	1734/663/123/140000	1.13/3.21/4.77	1.13/4.34/9.11	Lateritic Topsoil/Sand/Weathered

						Basement/Fresh Basement
48	4	QH	2167/637/142/160000	0.984/2.16/5	0.984/3.14/8.14	Lateritic Topsoil/Sand/Weathered Basement/Fresh Basement
49	4	QH	2568/841/234/230000	0.537/3.91/6.16	0.537/4.45/10.6	Lateritic Topsoil/Sand/Weathered Basement/Fresh Basement
50	4	KH	196/533/57.3/36826	0.171/5.13/5.47	0.171/5.3/10.8	Topsoil/Sand/Weathered Basement/Fresh Basement
51	4	QH	896/223/30.1/51008	1.67/4.83/6.9	1.67/6.5/13.4	Lateritic Topsoil/Clayey Sand/Weathered Basement/Fresh Basement
52	4	QH	453/112/11.5/19378	0.832/5.12/6.56	0.32/5.95/12.5	Lateritic Topsoil/Clayey Sand/Weathered Basement/Fresh Basement
53	4	QH	4750/788.9/192.8/3130	1.725/4.025/7.123	1.725/5.75/12.87	Lateritic Soil/Compacted Sand/Weathered Basement/Fresh Basement
54	4	QH	2336/1413/283/110000	0.943/3.78/16.8	0.943/4.72/21.5	Lateritic Topsoil/laterite/Weathered Basement/Fresh Basement
55	5	QQH	8371/3402/868/273/230000	0.511/1.53/7.01/8.02	0.511/2.04/9.04/17.1	Lateritic Topsoil/Lateritic Sand/Sand/Weathered Basement/Fresh Basement
56	5	QQH	9348/1021/181/102/57133	0.6/2.03/8.84/12.5	0.6/2.63/11.5/23.9	Lateritic Topsoil/Laterite, Fracture Basement/Weathered Basement/ Fresh Basement
57	5	KQH	2789/7214/330/90.9/94405	0.731/0.621/5.93/6.34	0.731/1.35/7.28/13.6	Lateritic Topsoil/Lateritic Sand/Weathered Basement/Fresh Basement
58	4	QH	3065/115/30.9/40856	1.55/5.55/9.05	1.55/7.1/16.2	Lateritic Topsoil/Clayey Sand/Weathered Basement/Fresh Basement

59	4	QH	4863/1107/240/210000	1.18/2.6/13.2	1.18/3.78/16.9	Lateritic-Topsoil/Laterite/Weathered Basement/Fresh Basement
60	4	QH	5197/803/185/6824	0.558/2.33/55.4	0.558/2.89/58.3	Lateritic Top/Sand/Weathered Basement/Fresh Basement
61	5	QQH	6538/1917/178/55.4/75525	0.382/1.74/5.56/8.5	0.382/2.12/7.68/16.2	Lateritic Topsoil/laterite/Sandy Clay/Weathered Basement/Fresh Basement
62	5	KQH	1919/3969/75.8/30.6/17680	0.969/1.51/10.8/11.5	0.969/2.48/13.2/24.7	Topsoil/Laterite/Weathered Basement/Fresh Basement
63	4	QH	35517/3644/602/49563	0.668/2.68/67.8	0.668/3.35/71.1	Lateritic Topsoil/Laterite/Fractured Basement/Fresh Basement
64	4	QH	4331/1460/250.6/86470	0.4091/2.045/20.28	0.4091/2.454/22.73	Lateritic Topsoil/Laterite/Weathered Basement/Fresh Basement
65	3	H	1719/244/170000	2.44/14.9	2.44/17.3	Lateritic-Topsoil/Weathered Basement/Fresh Basement
66	4	QH	4964/1839/659/95799	1.39/1.64/21	1.39/3.03/24	Lateritic Topsoil/laterite/Fractured Basement/Fresh Basement
67	5	HKH	5481/336/202/99.5/3892	0.525/0.577/5.45/6.65	0.525/1.1/6.55/13.2	Lateritic Topsoil/Sand/Weathered Basement/Fresh Basement
68	4	QH	3806/580.2/225.7/158477	0.5325/1.287/15.53	0.5325/1.819/17.35	Lateritic Topsoil/Sand/Weathered Basement/Fresh Basement
69	5	KQH	1603/3498/621/330/82485	0.557/0.604/4.39/20.1	0.557/1.16/5.55/25.7	Lateritic Topsoil/Laterite/Fractured Basement/Fresh Basement
70	3	H	413.4/182.9/9565	0.6395/16.41	0.6395/17.05	Topsoil/Clayey-Sand/Fresh Basement

71	4	KH	391/1425/51.5/745	0.843/0.567/23.9	0.843/1.41/25.3	Topsoil, Laterite/Weathered Basement/Fracture Basement

Fig. 3 Geoelectric section model for VES 1 to VES 28 along the study area

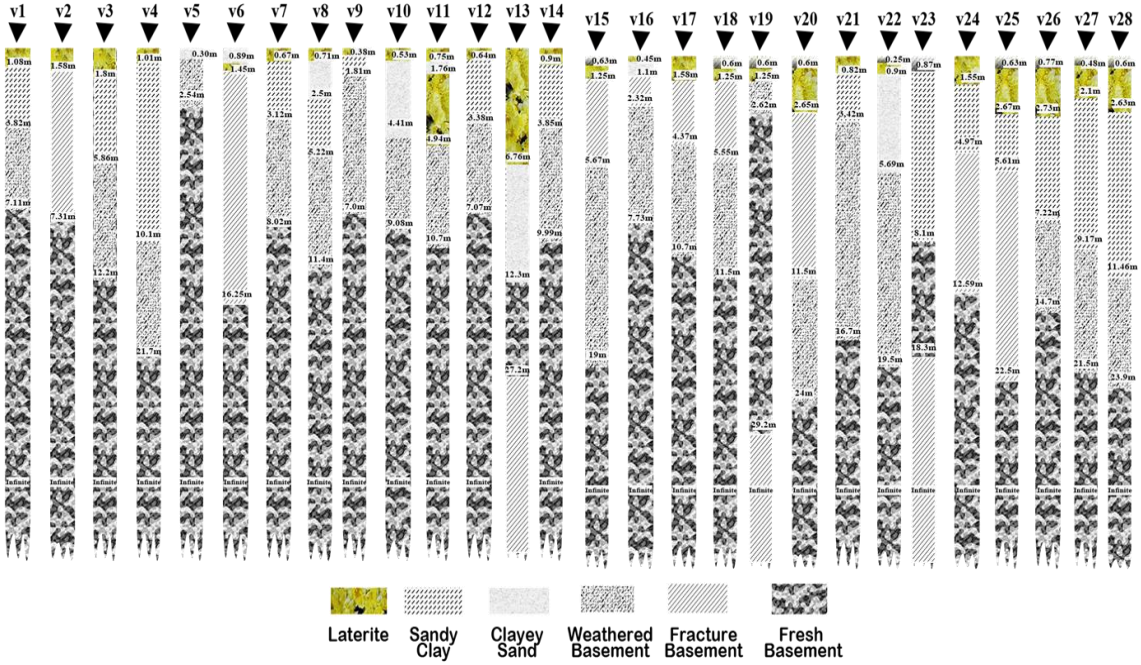

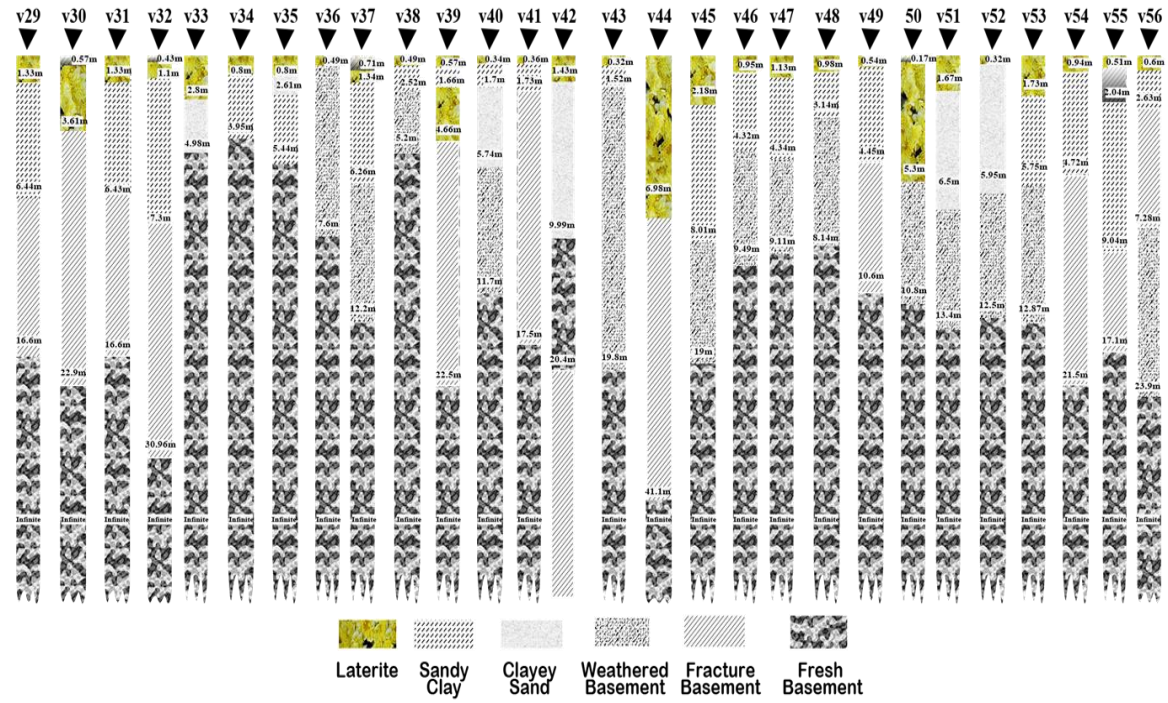

Fig. 4 Geoelectric section model for VES 29 to VES 56 along the study area

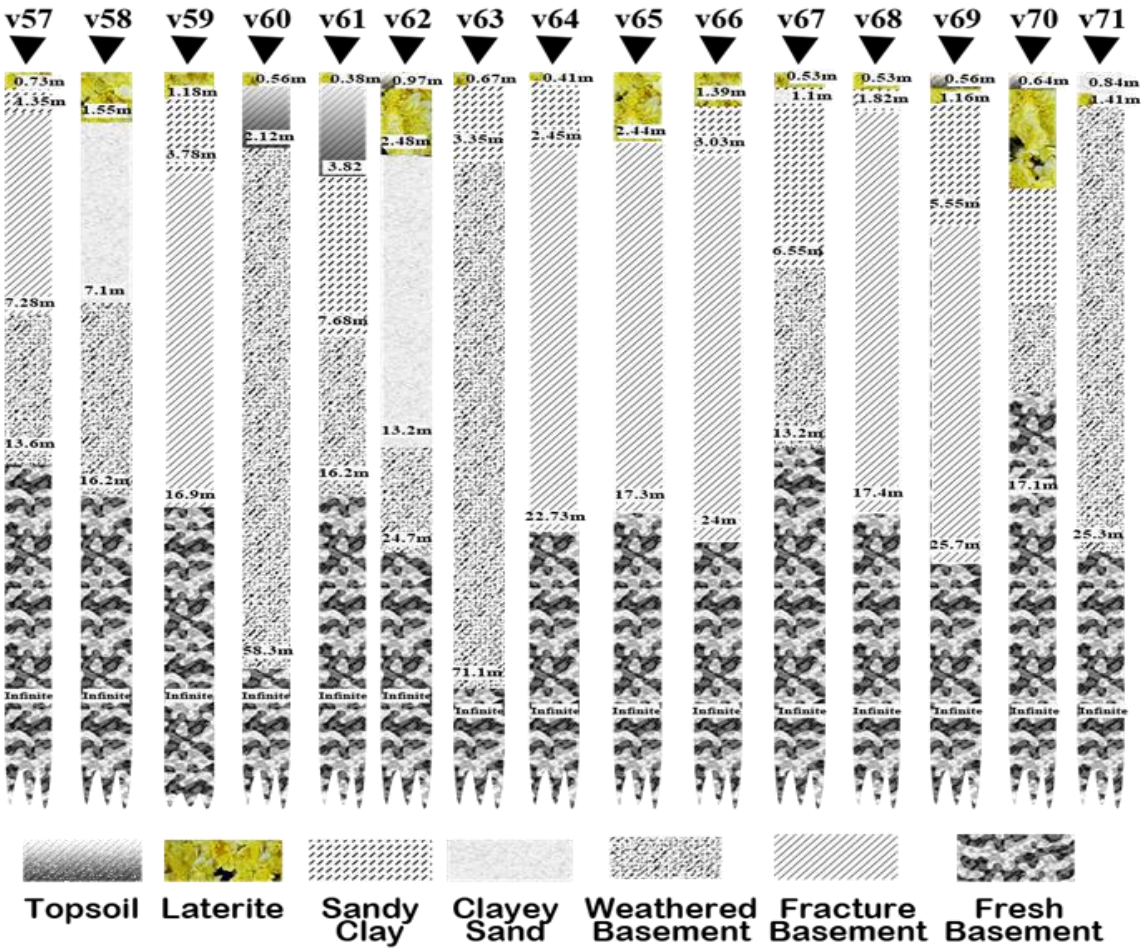

Fig. 5 Geoelectric section model for VES 57 to VES 71 along the study area

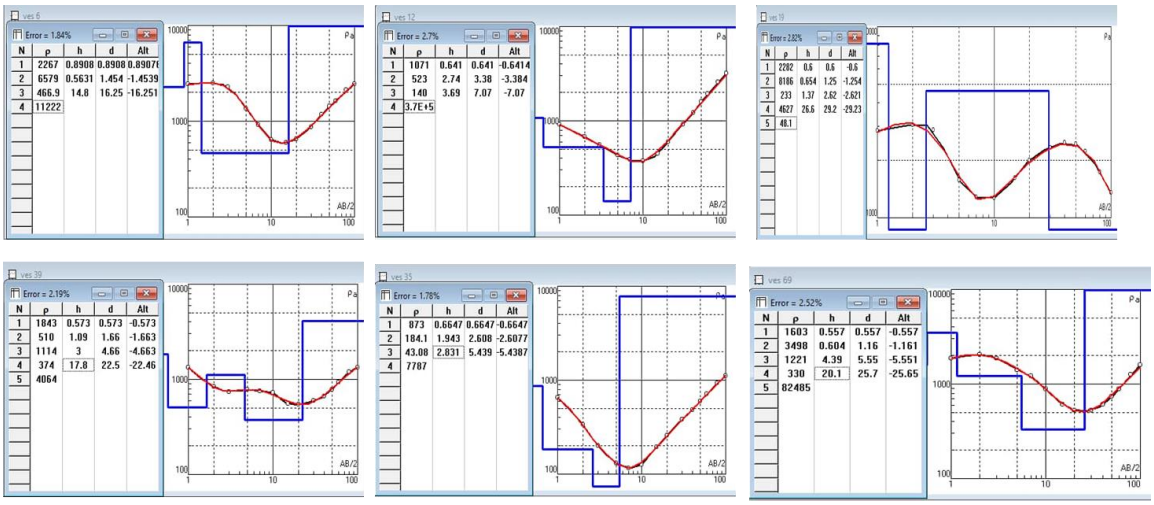

Fig. 6 Sample of IPI2WIN Resistivity-depth Plot

Moreover, the geoelectric section, as shown in Figures 3 to 5, derived from the VES interpretations, delineates zones of weak subgrade materials and saturated formations that correspond spatially with observed pavement failures. Areas exhibiting thin lateritic cover and thick clayey or sandy-clay sublayers show poor bearing capacity, particularly in sections where

drainage is inadequate. Also, sections with thicker lateritic overburden and shallow, compacted bedrock display higher resistivity values and are relatively stable with minimal evidence of deformation.

Discussion

The electrical resistivity results provide insight into the mechanisms controlling pavement performance along the Shao-Malete Road by revealing the spatial distribution of competent and failure-sensitive subsurface units. The interpretation highlights how variations in resistivity, layer thickness, and basement geometry govern road stability under seasonal loading and moisture fluctuations. The widespread presence of lateritic topsoil indicates that the area is underlain by predominantly tropical residual soils derived from the intense weathering of the crystalline basement complex. However, lateritic materials are generally competent when dry and compacted; their mechanical strength deteriorates rapidly under high moisture conditions due to dispersion of fine-grained particles and loss of cohesion. Areas where the lateritic layer is less than 1 m thick, notably at VES 6-10, 12, 14, 16, 21, and adjacent locations, show reduced bearing capacity and are more prone to surface deformation and pavement cracking. These findings confirm that a thin lateritic cover is a key factor contributing to road instability, particularly when sub-base reinforcement is inadequate.

The intermediate clayey-sand and sandy-clay layers, with thicknesses ranging from 0.5 m to 11 m, further exacerbate the subgrade's instability. Their moderate resistivity values reflect a variable mixture of sand and clay minerals, the latter of which are highly susceptible to swelling and shrinkage cycles. During the rainy season, these layers absorb moisture, expand, and lose strength, thereby inducing upward stress on the pavement structure. Previous studies indicate that clay-rich tropical soils typically exhibit low resistivity due to high moisture retention and ionic pore fluids, conditions that promote swelling, shrinkage, and loss of shear strength (Adenika et al., 2018). Road sections where these clayey formations occur directly beneath thin lateritic cover, such as at VES 5, 11, 22, 35, 42, 51, 52, 58, and 62, correspond to zones of severe pavement deterioration. Additionally, the sandy-clay layers often serve as conduits for water infiltration, promoting subsurface saturation, reducing load-bearing capacity, and accelerating pavement collapse. This mechanism is consistent with the moisture-induced subgrade failure observed in tropical geotechnical environments (Adenika et al., 2018).

At deeper depths, the weathered and fractured basement layers exert substantial control over the overall road performance. In zones where the weathered basement is thick and poorly compacted, particularly at VES 7-12, 14, 16, 21, 27, and 35-38, it exhibits low geotechnical competence and a higher tendency for differential settlement and subsurface void formation. While the weathered basement is thin and overlies shallow fresh bedrock, the subsurface exhibits greater compactness and enhanced bearing capacity. The variable depth to fresh basement, ranging from 2.5 to 58 m, indicates irregular structural features, such as fractures and fault zones, within the crystalline basement, which serve as pathways for groundwater infiltration. These discontinuities accelerate subsurface weakening and promote localized failure, particularly where they coincide with clayey subgrade materials.

Therefore, the analysis shows that road performance along the Shao–Malete corridor depends on the combined effects of lateritic cover thickness, moisture-sensitive subgrade materials, and basement structural variability. By differentiating stable from failure-prone zones based on resistivity characteristics, this study highlights the importance of geophysical investigations as a decision-making tool in road engineering. It emphasises the need for geophysical pre- and post-assessment in highway engineering to accurately identify weak zones before construction or rehabilitation. Understanding the subsurface resistivity structure thus provides a scientific

basis for designing more durable, geotechnically sound, and sustainable road networks across similar basement-complex terrains.

Conclusion and Recommendation

This study demonstrates the effectiveness of the Electrical Resistivity Method using the Vertical Electrical Sounding (VES) technique in identifying subsurface conditions responsible for recurrent road failures along the Shao-Malete Road in Kwara State. The interpreted resistivity models delineate a layered subsurface comprising lateritic topsoil, clayey sand, sandy clay, and a weathered basement overlying the fresh basement. Road sections underlain by thin or discontinuous lateritic cover and shallow, low-resistivity clay-rich layers were consistently associated with observed pavement distress. These low-resistivity materials indicate high moisture retention, poor drainage, and reduced bearing capacity, which promote deformation, settlement, and surface deterioration under traffic loading.

The geophysical investigation provides a clear basis for targeted engineering interventions. In sections where resistivity data indicate thick clayey or weathered layers, subgrade improvement using crushed stone, lime or cement stabilization is recommended to enhance strength and reduce moisture sensitivity. While, areas with relatively higher resistivity lateritic materials may require minimal stabilization but improved drainage to prevent water infiltration. The integration of surface and subsurface drainage systems is particularly critical in zones characterized by low resistivity, reflecting water-saturated and swelling-prone soils. Integrating geophysical data with geotechnical and geochemical analyses, along with good construction materials, will provide a more complete framework for sustainable road construction in the region.

Although the VES method successfully characterized vertical resistivity variations, its one-dimensional inversion assumes laterally homogeneous layers. It may not fully capture complex geological features such as lateral facies changes, fractures or localized weak zones. To improve the reliability of subsurface assessments, future studies should incorporate 2D and 3D resistivity imaging, supported by laboratory-based geotechnical testing, to provide more robust data for designing durable and sustainable road infrastructure in the study area and similar geological settings.

References

Adagunodo T. A., Adeniji, A. A., and Okeniyi, E. T. (2025). Causes and Possible Solutions to Road Failure in Nigeria. Lecture Notes in Civil Engineering, 55–65. https://doi.org/10.1007/978-981-96-1627-5_5

Ademila, O. (2022). Engineering Geophysical Investigation of Oka-Isua-Ibillo Highway Failure; Remedy and Road Sustainability in Nigeria. JOURNAL of SCIENTIFIC RESEARCH, 66(01), 41–52. https://doi.org/10.37398/jsr.2022.660105

Adenika, C. I., Ariyibi, E. A., Awoyemi, M. O., Adebayo, A. S., Dasho, O. A., and Olagunju, E. O. (2018). Application of geophysical approach to highway pavement failure: a case study from basement complex terrain southwestern Nigeria. International Journal of Geo-Engineering, 9(1). https://doi.org/10.1186/s40703-018-0076-0

Agati, J., Sani, S., Bernard, R., David, E., and Mangai, C. (2023). Causes of failure of Nigerian roads: A review. 8(2), 217–223. https://doi.org/10.30574/wjaets.2023.8.2.0079

Agbo, S., Akeem A., and Kolo, M. (2024). GEOTECHNICAL INVESTIGATION OF ROAD FAILURE ALONG ABUJA- LOKOJA ROAD. Deleted Journal, 2(1), 1–1. https://doi.org/10.5455/njeas.188354

Ajadi, J., Yusuf, M., Omolaiye, G. E., Adam, S. B., and Alade, A. D. (2025). Evaluation of groundwater resources using remote sensing and GIS techniques within Kwara State University, Malete, Nigeria. Discover Geoscience, 3(1). https://doi.org/10.1007/s44288-025-00244-0

Akingboye, A. S. (2025). Electrical and seismic refraction methods: Fundamental concepts, current trends, and emerging machine learning prospects. Discover Geoscience, 3(1). https://doi.org/10.1007/s44288-025-00169-8

Alao, J. O., Lawal, K. M., Dewu, B. B. M., and Raimi, J. (2024). Detection of shallow underground targets using electrical resistivity tomography and the implications in civil/environmental engineering. Discover Geoscience, 2(1). https://doi.org/10.1007/s44288-024-00058-6

Alao, J. O., Lawal, K. M., Dewu, B. B. M., and Raimi, J. (2025). Near-surface seismic refraction anomalies due to underground target models and the application in civil and environmental engineering. Physics and Chemistry of the Earth, Parts A/B/C, 138, 103845. https://doi.org/10.1016/j.pce.2024.103845

Alsharahi, G., Filali Bouami, M., Faize, A., Louzazni, M., Khamlichi, A., and Atounti, M. (2021). Contribution of analysis and detection the risks appearing in roads using GPR method: A case study in Morocco. Ain Shams Engineering Journal, 12(2), 1435–1450. https://doi.org/10.1016/j.asej.2020.10.014

Bamidele, O. E. and Omojemite, K. T. (2025). PRE-CONSTRUCTION GEOELECTRIC INVESTIGATION OF ICT ROAD, FEDERAL UNIVERSITY OYE-EKITI, EKITI-STATE, SOUTHWESTERN NIGERIA. JOURNAL of INNOVATION SCIENCE and TECHNOLOGY, 4(1). https://jist.fuoye.edu.ng/index.php/jist/article/view/106

Fajana, A., Jolayemi, M. D., Tsado, T., and Taiwo, E. A. (2024). Geoelectric Characterization of the Subsurface Road Pavement Failures Along Itapa-Ikole Highway, Southwestern, Nigeria. Savanna Journal of Basic and Applied Sciences, 6(2). https://sjbas.com.ng/journal/052908Fajana%20et%20al.pdf

Oluyemoh A. O., Omolaiye, G. E., Ajadi J., and Adam, S. B. (2025). High-resolution aeromagnetic mapping for subsurface investigation to support smart city infrastructure planning at Kwara State University, Malete. Modeling Earth Systems and Environment, 11(5). https://doi.org/10.1007/s40808-025-02565-y

Omolaiye, G. E., Oniyangi, K. A., ISSA, T. A., and Adam, S. B. (2024). Subsurface investigation for pre-foundation study utilizing integrated geophysical and geotechnical methods, UNILORIN campus. Discover Geoscience, 2(1). https://doi.org/10.1007/s44288-024-00103-4

Omolaiye, G. E., Adam, S. B., Issa, T. A., Yusuf Magaji, Oniyangi, K. A., Ajadi, J., Olatunji, S., Oluyemoh, A. O., and Ojulari B. A. (2025). Geophysical investigation of groundwater potential and aquifer properties using ground magnetic and vertical electrical sounding at the University of Ilorin, Nigeria. Modeling Earth Systems and Environment, 11(3). https://doi.org/10.1007/s40808-025-02383-2

Oyinkuro O. A. and Wilson, O. A. (2025). Characterization of Sub-Soil Corrosion Potential Using Electrical Resistivity Method across the Niger Delta University Campus, Bayelsa State, Southern Nigeria. International Journal of Recent Engineering Science, 12(2), 20–27. https://doi.org/10.14445/23497157/ijres-v12i2p103

Paweł, P., Andrzej, K., Akinniyi, A., Tomasz, D., Anna, M., and Miroslaw, Z. (2025). Identification of anomalies under the road surface using GPR. PRZEGLĄD ELEKTROTECHNICZNY, 1(3), 109–112. https://doi.org/10.15199/48.2025.03.26

Rahimi, M., Wood, C. M., and Kallivokas, L. F. (2024). A comparative study of using geophysical methods for imaging subsurface voids of various sizes and at different depths. Engineering Geology, 341, 107711–107711. https://doi.org/10.1016/j.enggeo.2024.107711

Rasol, M., Pais, J. C., Pérez-Gracia, V., Solla, M., Fernandes, F. M., Fontul, S., Ayala-Cabrera, D., Schmidt, F., and Assadollahi, H. (2022). GPR monitoring for road transport infrastructure: A systematic review and machine learning insights. Construction and Building Materials, 324, 126686. https://doi.org/10.1016/j.conbuildmat.2022.126686

Yusuf, M., Omolaiye, G. E., Oluyemoh, A. O., Ajadi, J., Adam, S. B., Egbeyale, G. B. and Alade, A. D. (2025). Hydrogeological assessment of groundwater potential zones using remote sensing, geographical information system (GIS) and aeromagnetic data at Kwara State University, Malete, Nigeria. Discover Water, 5(1). https://doi.org/10.1007/s43832-025-00273-3